Multiproton final states in positive pion absorption below the $\Delta(1232)$ resonance

R. A. Giannelli, B. G. Ritchie, J. M. Applegate, E. Beck,* J. Beck,† and A. O. Vanderpool
Arizona State University, Tempe, Arizona 85287-1504

C. L. Morris and M. Rahwool-Sullivan
Los Alamos National Laboratory, Los Alamos, New Mexico 87545

M. K. Jones,‡ R. D. Ransome, and M. Yadav
Rutgers University, Piscataway, New Jersey 08855

D. L. Watson
University of York, York YO10 5DAD, United Kingdom

K. O. Oganesjan§ and E. A. Pasyuk‖
Joint Institute for Nuclear Research, Dubna, Moscow Region 141980, Russia

F. F. Guber and A. I. Reshetin
Institute for Nuclear Research of the Russian Academy of Science, Moscow 117312, Russia
(Received 9 July 1998; revised manuscript received 19 July 1999; published 20 April 2000)

Inclusive cross sections for positive pion absorption leading to final states including two or more protons have been measured with a large solid angle detector for incident pion energies from 30 to 135 MeV for targets with $A=2-208$. The mass dependences for the inclusive $(\pi^+,2p)$, $(\pi^+,3p)$, and total absorption cross sections for multiproton final states were found to be proportional to A^n with $n\approx 0.5$. These cross sections also were observed to have an energy dependence at energies below 150 MeV reflective of the importance of the $\Delta(1232)$ resonance, similar to that observed for $\pi d\rightarrow pp$. The inclusive cross sections for $(\pi^+,4p)$ were found to be less than 10 mb for all targets at all energies. Estimates were also obtained for cross sections for pion absorption leading to $2p1n$ and $3p1n$ final states. Quasideuteron absorption contributions increase slowly with *A*, and the energy dependence of those contributions mirrors that for $\pi d\rightarrow pp$. The data obtained here for multiproton final states indicate that a significant fraction of absorption events, increasing with *A*, most likely arises from final states containing fewer than two protons.

PACS number(s): 25.80.Ls, 25.80.Hp

I. INTRODUCTION

Pion absorption has been the subject of numerous studies throughout the periodic table for a range of pion energies below, above, and at the energy of the $\Delta(1232)$ resonance. As detailed in several recent reviews of the topic [1–3], this process represents an important component of pion-nucleus reactions, accounting for not less than one-tenth of the total pion-nucleus cross section at energies below 500 MeV.

Until very recently, definitive measurements of the relative strengths of the different multinucleon final states for nuclei with $A>2$ did not exist because these previous measurements typically were limited in solid angle coverage. In general, early experiments (for example, Burger *et al.* [4]) determined total absorption cross sections by extrapolating differential cross sections from small solid angle detector measurements. These extrapolated measurements hinted that the absorption process was not limited to two-nucleon or quasideuteron absorption (QDA), but also included multinucleon absorption processes that accounted for at least 20% for the absorption cross section in nuclei with $A>6$. However, because of the limited solid angle coverage of these initial studies, the estimates were ambiguous, and the relative strengths of different absorption mechanisms were left undetermined. Hence, although a large amount of data exists for the total pion absorption cross sections, there are few data that allow the determination of the individual components of the absorption process.

Recently, larger solid angle detectors have begun to investigate the relative strengths of the different multinucleon reaction mechanisms in pion absorption for pion energies above and at resonance [5–23]. In very light nuclei such as ^{6}Li [5,6,14,17] and the helium isotopes [12,13,15,18,19] these large solid angle coverage studies have been especially successful, helped in part because of the relatively small number of possible final states allowed for modeling. With these newer studies, progress has been made in refining our

*Present address: Phillips Laboratory, Kirkland AFB, Albuquerque, NM 87117-5776.
†Present address: Department of Physics, University of Washington, Seattle, WA 98195-4290.
‡Present address: Department of Physics, College of William and Mary, Williamsburg, VA 23187-8795.
§Deceased.
‖Present address: Department of Physics and Astronomy, Arizona State University, Tempe, AZ 85287-1504.

knowledge of the mechanisms involved in pion absorption as well as the role of initial and final state interactions in the process. For instance, the helium isotope studies [12,13,15,18,19] suggest that three-particle final states reflect QDA with initial state interactions as well as a distribution of the energy and momentum for the three nucleons reflective of phase space.

However, a thorough systematic study of the energy and mass dependences has yet to be done below resonance. While there have been measurements of pion absorption cross sections for energies below the peak of the $\Delta(1232)$ resonance, those studies have left large gaps in the energy and nuclear mass dependences. With respect to improving understanding of the absorption process, these gaps are of concern since the mean free path of the pion changes markedly with increasing pion energy below the $\Delta(1232)$ resonance.

We report here a study of positive pion absorption below the $\Delta(1232)$ resonance with incident pion energy steps of 15 MeV using a good sampling of the periodic table. The measurements, performed with the BGO Ball, a large (30/32 of 4π sr) solid angle detector, yield the mass and energy dependences of several multiproton final states, and provide estimates of the proportion of the total absorption cross section due to QDA at incident pion energies below the $\Delta(1232)$ resonance. By comparison with measured total pion absorption cross sections, observations concerning the role of final states with fewer than two protons can be made.

II. EXPERIMENT

The BGO Ball detector has been described elsewhere [5–8,10,11,24]; we review here the salient details for this experiment. The BGO Ball assembly consists of an array of 30 detector elements subtending a solid angle of approximately 30/32 of 4π sr. Each detector element consists of a plastic scintillator (providing an energy loss dE measurement) optically and physically coupled to a bismuth germanate (BGO) crystal (providing a total remaining energy E measurement). A single photomultiplier tube views each phoswich assembly. Each element is placed on 1 of 30 sides of a 32-sided truncated icosahedron. Two opposing faces are left open for passage of the beam and for introduction of target holders and beam monitor counters within a cavity in the interior of the Ball.

The experiment was performed in the Clinton P. Anderson Meson Physics Facility (LAMPF) Low Energy Pion Channel [25]. Incident positive pion energies of 30, 45, 60, 75, 90, 120, and 135 MeV were used for primary data collection for all targets. (Additional data at 55 MeV were taken for ^{12}C.) Using the momentum slits of the channel, beam intensities were adjusted to maintain acceptable singles rates in the BGO Ball detector elements and beam monitoring devices described below. This generally resulted in pion beams with fluxes of less than 10^4 pions/s.

The pion beam passed through a lead collimator with an aperture 1 cm in diameter before passing through a ''beam halo veto'' scintillator positioned approximately 25 cm in front of the entrance port of the BGO Ball. This beam halo veto was a square piece of plastic scintillator 10 cm on a side and approximately 0.6 cm thick, subtending a solid angle of less than 1.5% of 4π sr with respect to the center of the BGO Ball detector. Inside the BGO Ball cavity, a 5-mm-square, 0.25-mm-thick ''target counter'' scintillator was placed just upstream in front of the target. The pion beam incident on the target was defined as an anticoincidence between the target counter and the beam halo veto. While particles could travel upstream from the target, miss the BGO Ball, and strike the beam halo counter, causing a false veto, the small solid angle subtended rendered the effects of such false vetoes insignificant.

Downstream of the BGO Ball array was a CsI crystal detector assembly, described in detail elsewhere [26]. Periodic sampling of the particles incident on the central CsI detector of this downstream array in anticoincidence with all the detectors in the BGO Ball allowed sampling of the beam composition to determine the pion fraction of the beam. This method of determining the pion fraction directly by energy loss particle identification is different from previous BGO Ball studies where the pion fraction was determined by time of flight through the channel for the incident pion beam.

Nine target materials were used for the measurements described here: deuterated polyethylene, ^{6}Li, ^{12}C, ^{27}Al, ^{58}Ni, and ^{208}Pb. This set of solid targets was chosen to encompass a broad range of atomic mass with materials which are stable over the duration of the experiment in an ambient air environment, though the ^{6}Li target was enclosed in a 25-μm-thick layer of Teflon to protect the lithium metal from oxidation. The atomic masses for the target materials increase in steps of approximately a factor of 2 from deuterium to lead, providing a reasonably smooth coverage in atomic mass A. Thickness uncertainties were less than 5% for all targets used in this experiment.

Two separate deuterated polyethylene targets were used, with thicknesses of 194 and 440 mg/cm^2. The deuterium content in these deuterated polyethylene targets provided both an absolute normalization for beam flux using the beam monitor counters and an energy calibration for the BGO crystals using the $\pi^+ d \rightarrow pp$ reaction. These $\pi^+ d \rightarrow pp$ measurements were made frequently during the data runs at each energy, including just before and immediately after target changes, to monitor any changes in beam content or detector function and to provide corrections for those changes. Absolute normalization was accomplished using the results of a parametrization of the $\pi^+ d \rightarrow pp$ cross section results [27].

The ^{6}Li, ^{12}C, ^{27}Al, and ^{58}Ni targets had thicknesses of 230, 279, 204, and 290 mg/cm^2, respectively. Two different ^{208}Pb targets were used, with thicknesses of 206 and 618 mg/cm^2. The different thicknesses for the deuterium and lead targets permitted comparisons of variation of event trigger rates and results obtained for the highest and lowest masses; no significant variation was observed.

The targets were positioned at the center of the BGO Ball cavity perpendicular to the incident pion beam and touching the target counter noted above. Positioning of the target within the BGO Ball interior cavity was accomplished by attaching each target to a paper tube mounted atop a hollow polyethylene shell. This thin polyethylene shell was in the

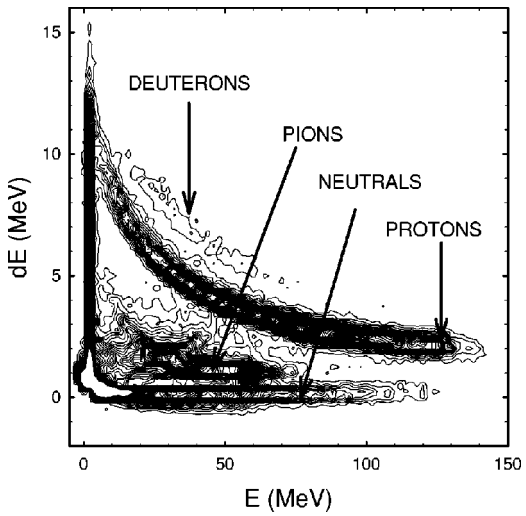

FIG. 1. Energy-calibrated pulse heights for the plastic scintillator (dE) versus the BGO scintillator (E) obtained by summing over all 30 counters for a data run on a ^{12}C target at 60 MeV. Bands for the major particle types are identified. Compare with Fig. 1 in Ref. [11].

shape of the missing downstream element of the truncated icosahedron. An ''empty'' target, formed by a paper tube and polyethylene shell identical to the normal target holders without any target material attached, was used to determine backgrounds related to the target holder assembly and target counter so that those contributions could be subtracted.

The hardware trigger for events for which results are reported here required two or more elements in the BGO Ball array hit by particles in coincidence with a valid beam on target event as described above and in anticoincidence with any hit in the central detector of the downstream array. As the hits in the BGO Ball could arise from the passage of any charged particles, neutrons, or gammas into the array, particle identification was required in order to ascertain the final state giving rise to the event trigger.

Particle identification and coincidence spectra with selected multiplicities were determined from the BGO Ball using E-dE spectra. The anode signals from the photomultiplier tubes on the BGO Ball array were time sliced to provide both dE (fast gated, 70–100 ns) and E (slow-gated, 500–600 ns) signals from the plastic scintillator and BGO crystals, respectively. A typical calibrated E-dE spectrum for an incident pion energy of $T_\pi = 60$ MeV is displayed in Fig. 1. Protons, pions, deuterons, and neutrals (either neutrons or gammas) have clearly distinct bands, as seen in the figure, resulting in reliable particle identification. The proton multiplicity was established by counting the number of protons detected in the BGO Ball. In this manner two-, three-, and four-proton inclusive coincidence spectra were measured.

Contributions from the polyethylene shell holding the target material were removed by subtracting a properly normalized spectrum obtained with the empty target shell at the same energy.

Typical resulting summed proton energy spectra for $2p$ and $3p$ events are illustrated by Figs. 2–6. These spectra are

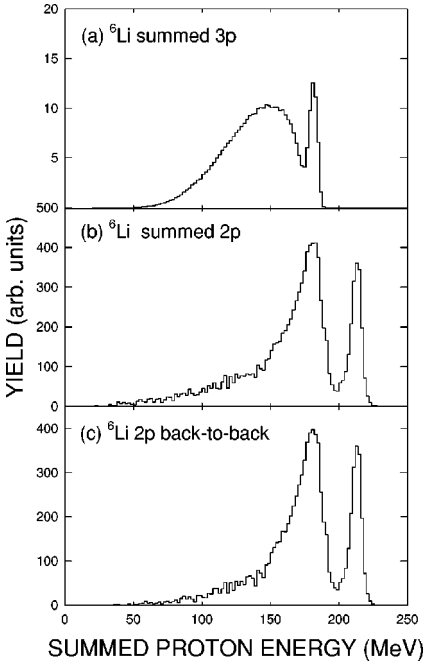

FIG. 2. Observed summed proton energy histograms for ^{6}Li at $T_\pi = 75$ MeV. (a) $3p$ spectrum. (b) $2p$ spectrum. (c) Summed energy spectrum given in (b) with events selected using ''back-to-back'' criteria discussed in Sec. IV C.

generated directly from absorption events using the trigger conditions, particle identification, and energy calibrations described above and, thus, are the most direct observations made in this series of measurements. Other than removal of empty target contributions, these spectra have none of the

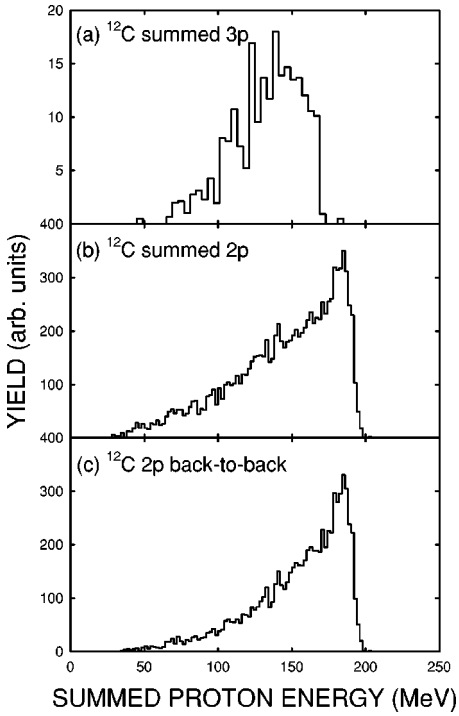

FIG. 3. Observed summed proton spectra for ^{12}C at $T_\pi = 75$ MeV. (a), (b), and (c) are as in Fig. 2.

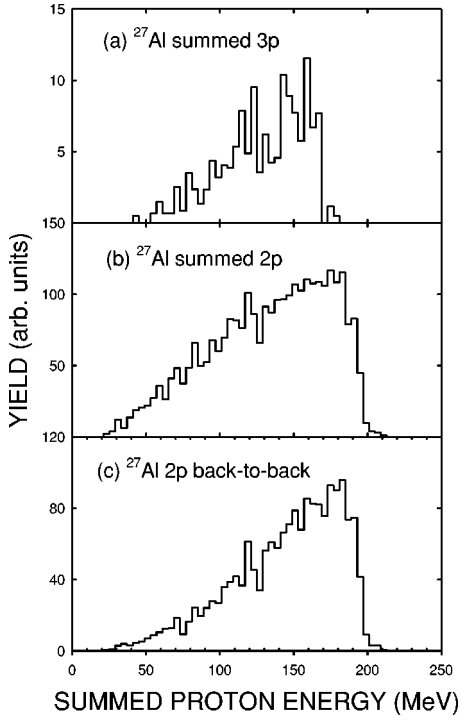

FIG. 4. Observed summed proton spectra for ^{27}Al at $T_\pi = 75$ MeV. (a), (b), and (c) are as in Fig. 2.

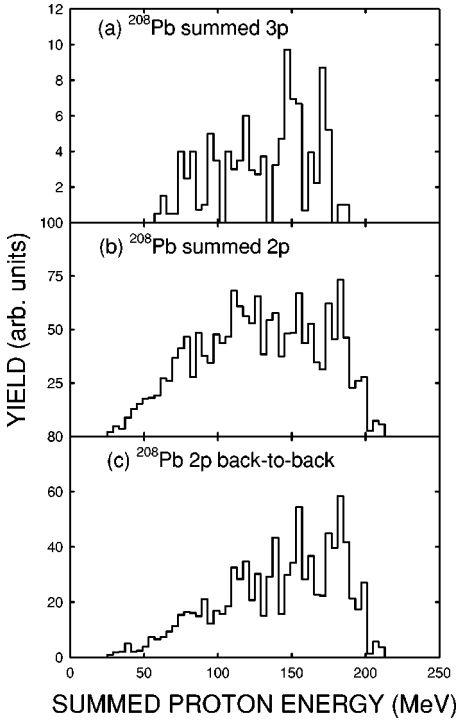

FIG. 6. Observed summed proton spectra for ^{208}Pb at $T_\pi = 75$ MeV. (a), (b), and (c) are as in Fig. 2.

corrections described in subsequent sections applied to them. Both the $2p$ and $3p$ summed proton energy spectra are seen to be similar to previously published spectra for these same nuclei [5–8,10,11,14,16,17,20,21].

The cross sections reported here are based only on events

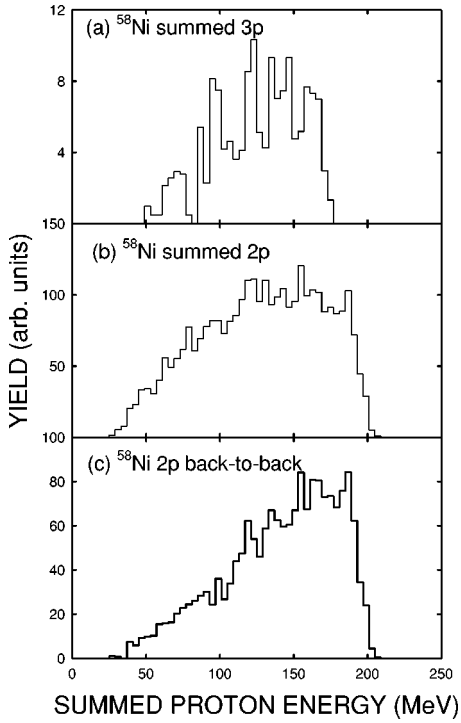

FIG. 5. Observed summed proton spectra for ^{58}Ni at $T_\pi = 75$ MeV. (a), (b), and (c) are as in Fig. 2.

where two or more protons were detected and there was no other detected particle. The large solid angle coverage allows rejection of most charged pions, but there is still the possibility that a pion can be missed for some reason. The contamination for missing a charged pion can be estimated from the (π^+,π^+pp) cross section. In addition, neutral pions may be observed from the two-gamma decay of the π^0. The contamination from missing a neutral pion can be estimated from the observed $(\pi^+,pp$ two neutral) cross section. Because the detection probability for high-energy photons is quite high (close to 100%) compared to neutrons (25% for 100 to 200 MeV neutrons and falling to zero for lower energy neutrons), most two neutral events are due to π^0 decays.

In each case we find the observed cross section to be less than 1% of the total $2p$ cross section, indicating an insignificant contamination level from unabsorbed pions. This is as expected. The total energy required to remove two protons from the nucleus and give both at least 15 MeV for detection is about 60 MeV, which is kinematically impossible at the lower energies and unlikely at the highest energy of 135 MeV. There is also no evident enhancement of the cross sections in the missing energy spectrum for the region where nonabsorption is possible, i.e., missing energies greater than 165 MeV.

Events in which two protons with sufficient energy to guarantee that the pion was absorbed were seen in coincidence with one or more neutrals, which are assumed to be primarily neutrons. The fraction of such events was small, as expected from the low neutron detection efficiency of the BGO crystals. Because the neutron detection efficiency is strongly energy dependent, the energy spectrum of the neu-

trons is not known, and the efficiency is not very well known, efficiency-corrected neutron yields would be insufficiently accurate to be of use. Thus, the analysis presented here is based solely on the energy information provided by the protons. The presence of neutrons in the final state was inferred from the results of the simulations of the observed proton energy spectra, as described below. As noted above, events where any neutral was detected were omitted from analysis.

While deuteron particle identification was clear, the estimated corrections for reaction losses for final states containing deuterons following pion absorption were very sensitive to details of target materials and interactions in the BGO Ball elements. The resulting corrections possessed sufficient ambiguity that cross sections for such final states could not be determined without very large uncertainties. Thus, cross sections for final states containing deuterons are not reported here. All events containing deuterons detected in the BGO Ball were excluded from the analysis presented here.

III. DEFINITION OF CROSS SECTIONS

The large number of cross sections presented in this work require categorization for clarity. Cross sections can be categorized according to which type(s) of analyses were performed. Here we outline the procedures used for extracting the categories of cross sections.

(a) Cross sections determined directly from the summed proton energy spectra observed with the BGO Ball are called *observed cross sections* σ_{obs}. Observed cross sections σ_{obs} thus represent the most basic of the cross section measurements undertaken here. Each σ_{obs} was calculated by normalizing the observed summed proton energy spectra to the total number of incident pions and the target areal density for the specific event trigger multiplicity selected, such as $2p$ or $3p$. Each σ_{obs} necessarily contains strength from higher proton multiplicity absorption events due to undetected protons.

(b) Using the event trigger described above, observed inclusive spectra for a given proton multiplicity (e.g., two protons) can include events with higher proton multiplicity (e.g., three or more protons) if the additional protons are not detected. Thus, the higher-proton-multiplicity final states contaminate the observed spectra for lower multiplicity events due to undetected protons in the latter spectra. These contaminations may be modeled and removed as described below. Cross sections for a given multiplicity which have had contamination due to higher-multiplicity events removed using the Monte Carlo simulations described below are referred to as *reduced cross sections*. For example, the reduced $2p$ inclusive cross sections result from events in which two and only two protons are in the final state, with no pion or deuteron but any number of neutrons in the final state.

(c) Some protons are missed due to inefficiencies of the experimental setup. For example, the BGO Ball misses approximately (2/32) of the 4π sr solid angle due to beam entrance and exit holes. Additionally, the nickel support cans subtend about 5% of the (30/32) of 4π sr covered by the BGO Ball. At all energies, final state protons lose energy due to nuclear reactions within the BGO detector elements and to scattering out of the crystals into the nickel support cans. This spreading of the proton band in the dE vs E plots can result in misidentification of protons. Also, protons, after energy losses within the target material, must have energies of at least 10 MeV or so to surmount the BGO Ball detection threshold. (This 10 MeV threshold is mainly due to the 0.05-mm-thick nickel window of the support cans.) Cross sections corrected for these inefficiencies utilizing the Monte Carlo phase space simulations of the BGO Ball response are called *corrected cross sections*.

(d) The combination of all three analyses described in (a), (b), and (c) results in the *inclusive cross sections*, wherein a particular number of protons in the final state, accompanied by any number of neutrons but no detected pion or deuteron, is selected. The $2p$, $3p$, and $4p$ inclusive cross sections are labeled σ^{2p}, σ^{3p}, and σ^{4p}, respectively.

(e) *Observed corrected cross sections* $\sigma_{obs,corr}$, derived from analyses (a) and (c), have been corrected for missing solid angle, etc., but have not had contributions subtracted due to higher multiplicity events using the Monte Carlo procedures described below. These cross sections are thus not affected by any assumptions inherent in the simulations other than those required to correct for missing solid angle and reaction losses.

(f) With analyses (a)–(c) and the phase space simulations described below, it was also possible to estimate exclusive cross sections for $2p1n$ and $3p1n$ final states, denoted σ_{excl}^{2p1n} and σ_{excl}^{3p1n}, respectively.

(g) The sum of the inclusive cross sections for a given target/energy combination provides a total cross section for pion absorption leading to multiproton final states for that target/energy combination. These are denoted as σ^{mp}.

(h) QDA cross section estimates σ^{QDA} had a different data reduction procedure explained in more detail below.

IV. ANALYSIS TECHNIQUES FOR SUMMED PROTON SPECTRA

A. Phase space simulations

Because BGO Ball measurements cannot determine the true final state nucleon multiplicity of every event owing to the inefficiencies and limitations described above, a Monte Carlo simulation of the BGO Ball's ability to differentiate between the different multinucleon final state spectra was used to analyze the data. The simulations model the exact geometry of the BGO Ball, target thicknesses, reaction losses, neutron detection efficiency, and the proton detection threshold. Details are given in Refs. [5] and [24]. These simulations enabled decomposition of the observed inclusive $(\pi^+,2p)$ and $(\pi^+,3p)$ cross sections for each target at each energy into reduced two- and three-proton cross sections.

The Monte Carlo simulations assumed that each pion absorption involving more than two nucleons took place on a quasifree nucleon cluster within the target nucleus, which then decayed according to the phase space (less the binding energy of the cluster) available to the multinucleon final states. This approach was used previously in unfolding measured spectra taken with the BGO Ball, and gives a reason-

able description of the observed inclusive spectra. As found in previous BGO Ball studies, any excitation energy assumed for the residual nucleus has only insignificant effects on the momentum and energy sharing, so excitations of the residual nucleus were ignored in the simulations here.

For the purposes of simulating the response of the BGO Ball to neutrons, procedures similar to those used in previous BGO Ball studies were used [5,6,11]. Neutrons with energies less than 30 MeV were assumed to be undetectable. For neutrons with energies greater than 100 MeV a constant 25% detection probability was assumed, with a linear interpolation used within the 30–100 MeV range.

Nearly 1500 phase space distributions for pion absorption on nucleon clusters for each of the target nuclei at each incident pion energy were generated. Final states simulated included the BGO Ball response for $2p0n$, $2p1n$, $2p2n$, $3p0n$, $3p1n$, $3p2n$, $3p3n$, and $4p0n$. The output of these simulations predicted the BGO response in terms of the observed $4p$, $3p$, and $2p$ inclusive spectra and angular distributions. For example, the simulation generated a given total number of $3p1n$ final state events. For each $3p1n$ event generated, tests were made on each of the particles to determine if the event would be detected by the BGO Ball as a $3p$ event (where the BGO Ball did not detect the neutron) or a $2p$ event (where the BGO Ball did not detect the neutron and one of the protons). These simulated $2p$ and $3p$ distributions from $3p1n$ events were then fitted to the respective observed $2p$ and $3p$ inclusive spectra simultaneously with other possible final states.

When fitting the simulated multinucleon $2pxn$ and $3pxn$ phase space distributions (where x is the number of neutrons emitted) to the measured $3p$ and $2p$ spectra, no unique solution for the combinations of the various final states was obvious, as a number of combinations were found to fit the observed spectra equally well. This ambiguity has been noted previously with respect to analyses of BGO Ball data (for example, Ref. [5]). However, the fits to the summed proton spectra are dominated by the contributions from final states with four or fewer nucleons, and, in particular, dominated by the $2p1n$ and $3p1n$ contributions. Most of the ambiguity in the fits lies in the degree to which the small strength which remains after the final states with four or fewer nucleons have been stripped away is apportioned to each of the higher multiplicity final states.

For each combination tried, the multinucleon portion of the higher-energy part of the spectra could not be fitted without a substantial contribution from $(\pi^+,2p1n)$ and $(\pi^+,3p1n)$ final states. The size of these two contributions resulted in generally unambiguous estimates of their strength. This permitted the determination of cross sections for exclusive absorption processes leading to only two protons, only two protons and one neutron, and only three protons and one neutron; these were extracted from the observed inclusive proton spectra, based on the strengths found in the simulations. At the same time, because of the overwhelming predominance of the $2p1n$ and $3p1n$ final states, the reduction of the higher residual nucleus excitation energy regions of the spectra (which corresponds to lower summed proton energy) into specific final states with more than one neutron was not possible without considerable ambiguity. That residual strength was generally relatively small.

$4p$ inclusive cross sections were measured, but no decomposition of those very small cross sections to specific exclusive final states was possible due to low statistics.

B. Deconvolution of inclusive spectra

The procedure for unfolding the measured spectra at each energy and for each target proceeded in the following manner. The observed $3p$ summed spectra were fitted first, and, as noted above, those spectra were generally dominated by $3p1n$ contributions. This fit to the observed $3p$ summed spectra consequently *fixed* the number of $3p$ and $3p1n$ events which could be present in the observed $2p$ summed spectra. The $4p$ contributions to the $2p$ and $3p$ distributions were fixed using the simulated response of the BGO Ball to a $4p0n$ final state and the observed $4p$ cross sections.

When fitting the observed $2p$ summed spectra, the total number of particles in each of the $2pxn$ simulated was a free parameter. The $2p1n$ contribution dominated the $2p$ spectra for all but ^{6}Li. The $2p0n$ phase space distribution fit was performed on the spectra below 100 MeV excitation energy because the higher multiplicity phase space distributions cannot reach the higher summed proton energy region due to the necessity of providing the extra separation energy for the additional nucleon. Furthermore, past BGO Ball results [11] indicate the the summed $2p$ spectra below 30–75 MeV excitation energy is dominated by QDA resulting in only $2p$ final states.

The resulting fits are illustrated in Figs. 7–11. Again, there is some ambiguity in the relative importance of contributions from final states representing absorption on five or more nucleons, but those contributions are small.

Except for ^{208}Pb, the second largest contribution to each observed $2p$ summed spectrum was the $3p1n$ phase space. In the ^{208}Pb spectra, a sizable fraction of the events was in the low summed proton energy region. Hence, a considerable amount of $2p2n$ and $2p3n$ phase space was needed to account for that part of the spectrum. Although the phase space fits to these regions are ambiguous, the strength at low summed proton energy could be evidence for contributions from final states with more than four protons.

C. QDA strength estimates

A long-standing question in the study of pion absorption concerns the importance of quasideuteron absorption. Though defined variously in the literature, the kinematical signature of QDA for positive pions is generally agreed to be the emission of two protons with equal and opposite momenta in the center-of-mass system (which we will call ''back-to-back'' henceforth) as if the process had occurred on a proton-neutron cluster. A further restriction usually applied is that the angular distribution of the outgoing protons be proportional to $\cos^2(\theta_{\mathrm{c.m.}})$ as in the free process. Absorption on quasideuterons deeply bound in the nucleus or absorption on a quasideuteron following excitation of the nucleus can result in QDA strength which follows the

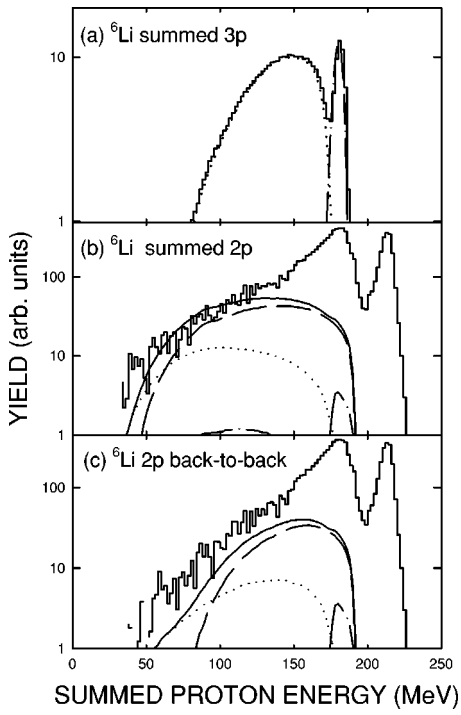

FIG. 7. Observed summed proton energy histograms with phase space simulations for ^{6}Li at $T_{\pi}=75$ MeV. The phase space contributions are $3p$ (denoted by dash-dotted line), $3p1n$ (dotted line), and $2p1n$ (long dashed line). The solid lines represent the sums of the phase space distributions. (a) $3p$ spectrum. (b) $2p$ spectrum. (c) Summed energy spectrum given in (b) with events selected using ''back-to-back'' criteria discussed in Sec. IV C.

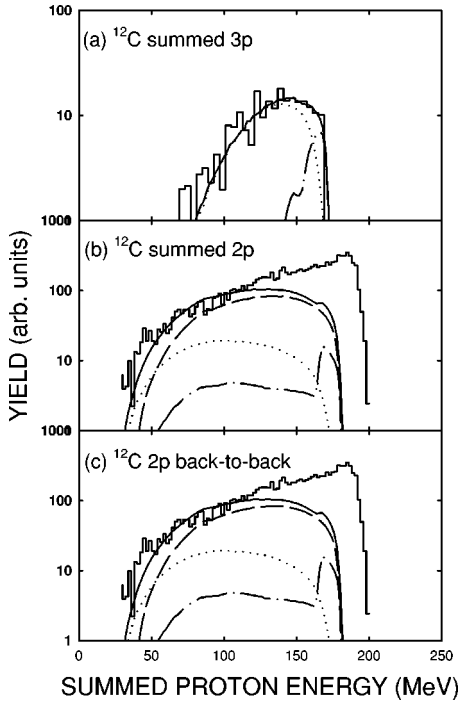

FIG. 8. Same as Fig. 7 for ^{12}C at $T_{\pi}=75$ MeV. (a), (b), and (c) are as in Fig. 7.

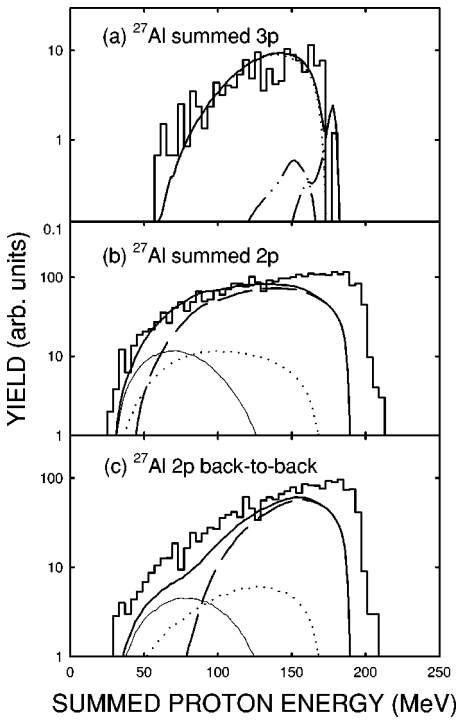

FIG. 9. Same as Fig. 7 for ^{27}Al at $T_{\pi}=75$ MeV. An additional phase space contribution from $3p2n$ is indicated by the thin solid line at lower summed proton energy. (a), (b), and (c) are as in Fig. 7.

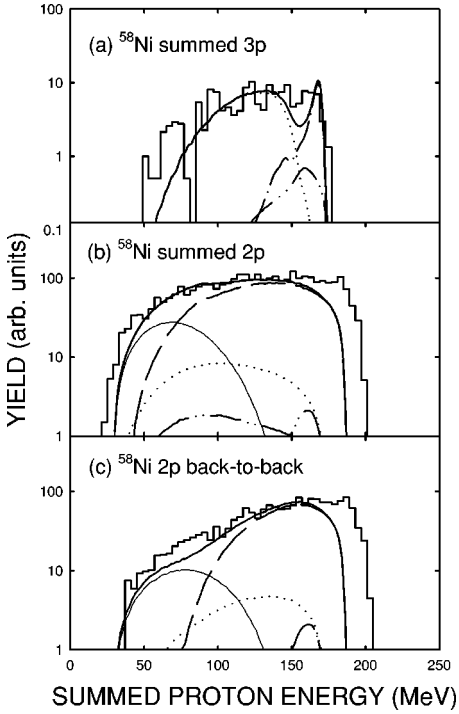

FIG. 10. Same as Fig. 7 for ^{58}Ni at $T_{\pi}=75$ MeV. An additional phase space contribution from $3p2n$ is indicated by the thin solid line at lower summed proton energy as in Fig. 9. (a), (b), and (c) are as in Fig. 7.

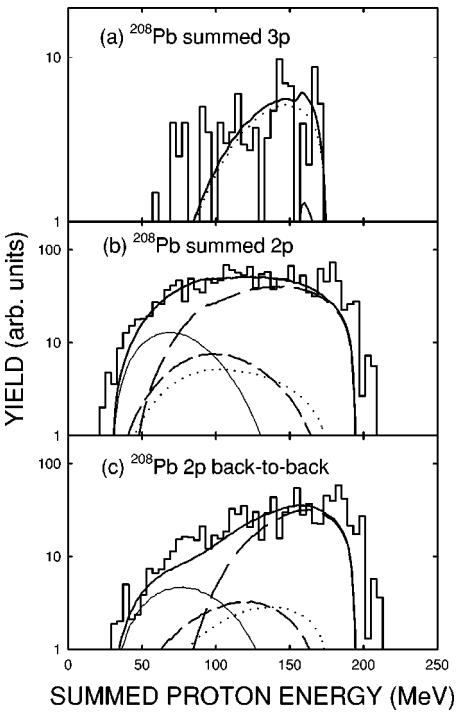

FIG. 11. Same as Fig. 7 for ^{208}Pb at $T_\pi = 75$ MeV. An additional phase space contribution from $3p2n$ is indicated by the thin solid line at lower summed proton energy as in Figs. 9 and 10. (a), (b), and (c) are as in Fig. 7.

$\cos^2(\theta_{\text{c.m.}})$ angular distribution but yields lower summed proton energy than in the case for ground state absorption.

We have modeled the presence of these two QDA components in our data in the following fashion. First, back-to-back tests were put on the two proton event data: histogrammed events were restricted to those events with a coincidence between a proton detected in one detector and another proton detected in one of the seven or eight contrapositioned detectors. The contraposition criterion was defined by the kinematics of the free $\pi^+ d \rightarrow pp$ reaction less the binding energy of the deuteron to the target nucleus. After fitting the phase space distributions to the full acceptance spectra as outlined in the previous section, the phase space distributions were regenerated with this same back-to-back restriction. These back-to-back distributions are seen in the lower portions of Figs. 2–6; the corresponding phase space distributions, with similar restrictions, are shown in the lower portions of Figs. 7–11

Next, the full angular acceptance of the BGO Ball was broken up to develop coarse angular distributions for the back-to-back events in the summed proton energy spectra. The full detector complement of the ball can be broken into ''rings,'' where each ring includes those crystals distributed in an azimuthal ring about an axis running along the incident pion beam through the BGO Ball; crystals in a ring thus fall along a common scattering angle. The back-to-back spectra from each ring of BGO Ball counters for ^{27}Al and ^{58}Ni at 75 MeV, typical of this analysis for other nuclei, are illustrated in the upper portions of Figs. 12 and 13. Also shown in those same figures are the phase space distributions sorted into

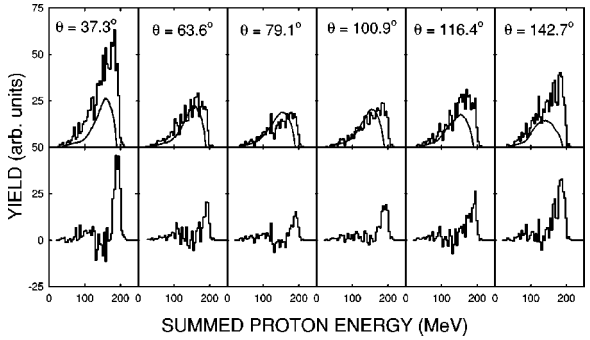

FIG. 12. Angular dependence of observed summed proton energy spectrum for ^{27}Al at $T_\pi = 75$ MeV with back-to-back cut imposed. The back-to-back cut is described in Sec. IV C. Also shown are the phase space distributions of Fig. 9, with the same back-to-back cut imposed scaled as discussed in the text. Spectra are shown for mean laboratory scattering angles of 37.3°, 63.6°, 79.1°, 100.9°, 116.4°, and 142.7°. The lower portion of each panel displays the spectrum for the particular scattering angle with the phase space contributions shown in the upper section of each figure normalized and removed as discussed in the text.

these rings using the same back-to-back and scattering angle requirements placed on the data.

The observed back-to-back angular distributions then were assumed to be made up of three components. One of the components was designated ''unperturbed QDA,'' in which two protons were emitted with a summed proton energy in excess of that feasible for two nucleons resulting from a three-nucleon phase space distribution in which one nucleon was undetected. This component should have an angular distribution proportional to $\cos^2(\theta_{\text{c.m.}})$, where the center-of-mass kinematics is appropriate for a deuteron being removed from the target nucleus. This unperturbed QDA contribution can be seen, for instance, in the bottom portions of Figs. 7–13 for summed proton energies above the $2p1n$ phase space prediction. A second QDA component was designated ''$2p1n$ QDA''; this component was that portion of the observed proton yield which followed the $\cos^2(\theta_{\text{c.m.}})$ behavior of unperturbed QDA but fell in the region dominated by the $2p1n$ phase space yield. The cross sections for these two components are designated by σ_{2p}^{QDA} and σ_{2p1n}^{QDA}, respectively.

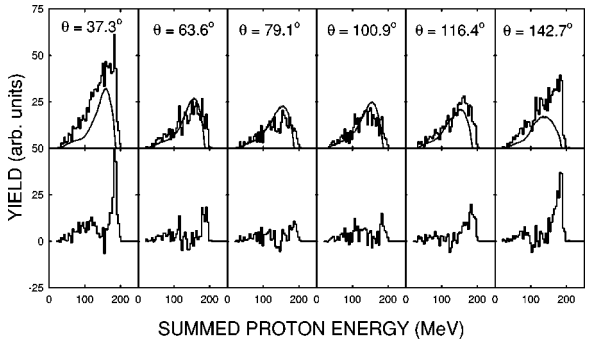

FIG. 13. Same as Fig. 12 for ^{58}Ni at $T_\pi = 75$ MeV using phase space distributions shown in Fig. 10.

The third component assumed was the contribution due to processes other than QDA. The phase space distributions were used in modeling this component. The angular distributions generated from the phase space distributions were fitted to the higher excitation portions of the summed proton energy data with the back-to-back tests for each row. These adjusted phase space distributions were then subtracted from the data. The adjustments of the phase space distributions for the various rows were subject to the constraint that the total yield from all rows was fixed by the phase space fits to the full angular acceptance, such as those shown in Figs. 7–11 for 75 MeV. Typically, the phase space distributions required enhancements by factors of 1.5–2 in the forward angles and reductions by factors of 0.6–0.8 in rows 3 and 4 (near 90°). These enhancements at forward angles and reductions at back angles are suggestive of the modifications of phase space discussed by Smith *et al.* for ^{3}He and by [28] and Simičević and Mateos [29] for the general case of absorption involving three nucleons, but are smaller in magnitude than found in those works.

Finally, cross sections were then calculated from the strengths of the unperturbed QDA and $2p1n$ QDA contributions to these fits by correcting the observed yield for missing solid angle and reaction losses, giving the cross sections σ_{2p}^{QDA} and σ_{2p1n}^{QDA}. Typical angular distributions for σ^{QDA} are shown in Fig. 14. The sum of σ_{2p}^{QDA} and σ_{2p1n}^{QDA} was assumed to estimate the total contribution due to QDA, denoted σ^{QDA}.

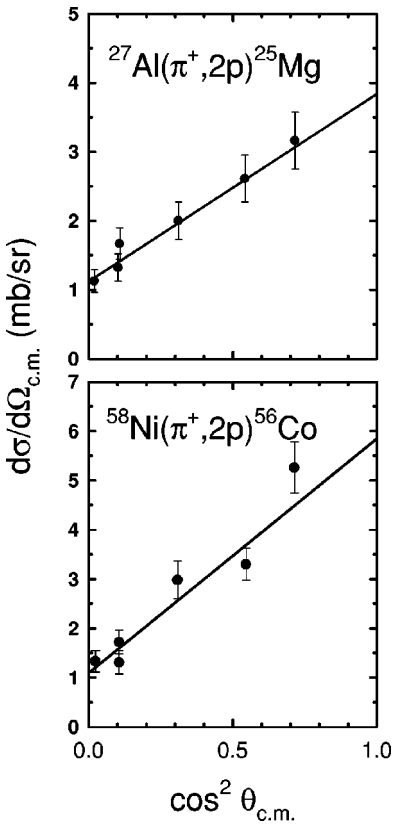

FIG. 14. QDA differential cross sections and fit for QDA $2p$ strength in ^{27}Al and ^{58}Ni at $T_\pi = 75$ MeV, as detailed in the text. Uncertainties shown represent estimates for normalization uncertainty and statistical uncertainty.

V. RESULTS

The inclusive pion absorption cross sections for various final states determined in this work using the techniques described above are given in Tables I and II. Statistical uncertainties for the inclusive $2p$ cross sections σ^{2p} range from a maximum of 8% for the 45 MeV data to below 4% for all other inclusive $2p$ cross sections listed in Tables I and II. Propagation of systematic uncertainties, including normalization uncertainty, yield uncertainties ranging from about 10–20% with the majority of cross sections having less than 15%. Conservatively, then, the absolute uncertainties may be assumed to be less than 25% for the σ^{2p} cross sections.

In Fig. 15 the inclusive $2p$ cross sections σ^{2p} from Table II are plotted. The figure includes previous BGO results for $2p$ cross sections at $T_\pi = 50$, 100, and 150 MeV corrected for contributions from higher multiplicity events. The cross sections shown in Fig. 15, with their associated uncertainties, were fitted to an exponential mass dependence $\sigma(T_\pi) \times A^n$ with an underlying smooth energy dependence. The exponent n for this mass dependence was determined to be 0.49 ± 0.02, with a χ^2 per degree of freedom of 1.4. This is roughly consistent with the mass dependence of $A^{0.4}$ found by Favier *et al.* [30] for the $(\pi^+,2p)$ inclusive reaction at 76 MeV. The rise with energy for these $2p$ cross sections is somewhat steeper than that seen for $\pi^+ d \rightarrow pp$, suggesting roles for components of the absorption reaction process other than QDA. The mass dependence for the total π^+ absorption reaction measured by Ashery *et al.* [31] was A^n with $0.75 \leqslant n \leqslant 1.0$, considerably higher than the $2p$ inclusive measurements reported here. Since, as will be seen below, the $2p$ component of the multiproton final states dominates the cross sections at these energies, this discrepancy points to underlying missing strength in the cross sections measured here, as discussed below.

Figure 16 illustrates the energy and mass dependence of the $3p$ inclusive cross sections σ^{3p} listed in Table II. Again, the figure includes previous BGO results for $3p$ cross sections at $T_\pi = 50$, 100, and 150 MeV, with the assumption that proton multiplicities above 3 contribute negligibly to the $3p$ inclusive cross sections; this assumption will be justified below. Statistical uncertainties for these $3p$ inclusive cross sections range from a maximum of 27% for the 45 MeV and 17% for the 30 MeV lead data to below 6% for all other $3p$ inclusive cross sections. Propagation of systematic errors yield overall uncertainties ranging from 15% to 44% with the majority having values less than 20%. A conservative estimate of the uncertainties for the data is 25%, except for the 45 MeV data where the uncertainties are around 45%.

These inclusive $(\pi^+,3p)$ cross sections increase by factors of about 10–40 for the energy range studied here. The exponential mass dependence A^n of these cross sections was determined in the same way noted above for the $2p$ data to be $n = 0.47 \pm 0.03$, with a χ^2 per degree of freedom of 1.6. This fit includes the results of Ransome *et al.* [5,6,8] at 50, 100, and 150 MeV, with the exception of the $3p$ inclusive lead cross sections which increased the χ^2 to 2.2.

TABLE I. Observed cross sections σ_{obs}^{2p}, σ_{obs}^{3p}, and $\sigma_{obs,corr}^{3p}$, as described in Sec. III. All cross sections are in mb. Uncertainties are discussed in the text.

Nucleus	T_π(MeV)	σ_{obs}^{2p}	σ_{obs}^{3p} / $\sigma_{obs,corr}^{3p}$
^{6}Li	30	17	0.30 / 0.78
	45	18	0.40 / 2.3
	60	20	1.1 / 2.5
	75	38	1.3 / 2.3
	90	57	2.7 / 4.9
	120	73	2.5 / 8.3
	135	122	3.2 / 17
^{12}C	30	23	0.28 / 0.72
	45	36	0.45 / 2.1
	55	43	1.5 / 3.3
	60	56	1.8 / 4.2
	75	72	2.2 / 4.4
	90	100	3.5 / 7.6
	120	144	4.9 / 17
	135	170	5.5 / 32
^{27}Al	30	38	0.51 / 1.4
	45	45	1.4 / 6.7
	60	68	3.6 / 8.4
	75	109	3.9 / 8.3
	90	155	7.5 / 17
	120	215	8.5 / 30
	135	250	6.3 / 46
^{58}Ni	30	42	0.71 / 1.9
	45	84	1.7 / 10
	60	94	6.2 / 14
	75	160	5.7 / 11
	90	196	8.8 / 19
	120	293	13 / 47
	135	338	9.8 / 71
^{208}Pb	30	78	2.2 / 5.8
	45	90	2.0 / 9.8
	60	127	7.8 / 16
	75	244	8.7 / 16
	90	277	10 / 22
	120	360	16 / 56
	135	407	24 / 65

Although the $4p$ summed spectra were not empty, these data are presented with a cautionary note. The observed $(\pi^+,4p)$ cross sections have values less than 1 mb and have uncertainties ranging from 50% to 100%, results consistent with previous BGO Ball results at 50, 100, 150, and 200 MeV [8], which reported that the $4p$ total cross sections were less than 0.5 mb even for the 200 MeV pions. The excitation functions for the $4p$ inclusive cross sections are displayed in Fig. 17. Systematically, these cross sections show an increase with pion energy and an increase with respect to nuclear mass, but all are much smaller than the $3p$ cross sections, usually by a factor of 20 or more. Thus, the contributions of these $4p$ cross sections to the $3p$ inclusive cross sections from earlier BGO Ball work noted above [8], when corrected for detection thresholds, missing solid angle, etc., are negligible.

Total multiproton absorption cross sections σ^{mp} were determined by adding the inclusive $2p$, $3p$, and $4p$ cross sections and assuming that higher proton multiplicities are insignificant. These absorption cross sections do not include contributions from final states which include detected deuterons or inclusive single proton final states. The total multiproton pion absorption cross sections inferred are shown in Fig. 18. The uncertainties in these cross sections are essentially those for the inclusive $2p$ cross sections; i.e., the uncertainties range from 10% to 20% with the majority of values having uncertainties less than 15%. A conservative estimate for the uncertainties for these total absorption cross sections leading to multiproton final states is 25%.

Again an exponential mass dependence was found for these total multiproton pion absorption cross sections, using A^n with $n=0.46\pm0.02$ with a χ^2 per degree of freedom equal to 1.3. The previous BGO Ball results at 50, 100, and 150 MeV of Ransome *et al.* [8] as noted above were also included in these fits and are consistent with the current results. The energy dependence reflects the general dominance of the $2p$ inclusive reactions for the region below resonance. This behavior also most likely reflects the underlying impact of the $\Delta(1232)$ resonance, just as is seen for the reaction $\pi^+d\rightarrow pp$. However, it is seen in the figures that, in all cases, the rise with energy in the multiproton cross sections is greater than in the case of $\pi^+d\rightarrow pp$.

Utilizing the phase space calculations, exclusive $(\pi^+,2p1n)$ and $(\pi^+,3p1n)$ cross sections were estimated. These reduced and corrected cross sections are listed in Table II. The uncertainties ranged between 15% and 20% for the $(\pi^+,2p1n)$ cross sections and between 20% and 25% for the $(\pi^+,3p1n)$ cross sections.

Unperturbed QDA cross sections are given in Table III. Statistical uncertainties in these cross sections are less than 10%. The overall uncertainties in these estimated cross sections are on the order of 20%. The σ_{2p1n}^{QDA} cross sections are also presented in Table III. As a result of the assumptions made in determining these cross sections, their uncertainties are on the order of 30%. Total QDA absorption cross sections estimates σ^{QDA} were derived from the sum of columns 3 and 4 in Table III and are listed in the last column. These σ^{QDA} cross sections are plotted in Fig. 19. The trend of these cross sections is very similar to that of the free $\pi^+d\rightarrow pp$ cross sections, which are also plotted in Fig. 19 for comparison. The statistical uncertainties in these total cross sections were less than 10% and propagation of systematic errors yield uncertainties of less than 40%.

VI. DISCUSSION

A. Comparisons with previous BGO Ball and LADS measurements

The results of the earlier BGO experiments [5,6,8] for the targets discussed here are consistent with the measurements reported here, with the inclusion of effects for the 25 MeV threshold used in those measurements. The earlier data at 50

TABLE II. Cross sections (in mb) for pion absorption leading to different multiproton final states as described in Sec. III. Uncertainties are as discussed in the text. Previous BGO Ball results from Ref. [8] are given for 50, 100, and 150 MeV for comparison, adjusted as noted in the text.

Nucleus	T_π (MeV)	σ^{2p}	σ^{2p1n}_{excl}	σ^{3p}	σ^{3p1n}_{excl}	σ^{4p}	σ^{mp}
^{6}Li	30	16	1.7	0.78	0.61	0	17
	45	14		2.3		0	16
	50	24		1.9			26
	60	18	1.5	2.1	1.7	0.4	20
	75	36	2.1	2.2	1.7	0.1	38
	90	50	7.5	4.7	3.1	0.2	55
	100	44		9.3			53
	120	61	7.0	7.9	5.9	0.4	69
	135	96	8.8	16	11	1	113
	150	52		14			66
^{12}C	12	22	6.4	0.70	0.65	0	23
	45	33		2.1		0	35
	50	45		3.1			48
	55	39		3.1	2.6	0.1	42
	60	50	31	3.7	3.4	0.2	54
	75	67	21	4.4	3.3	0.1	71
	90	90	41	7.2	6.0	0.2	97
	100	88		10			98
	120	121	37	16	12	0.6	138
	135	128	33	29	13	2.0	159
	150	92		21			113
^{27}Al	30	36	14	1.4	1.1	0	37
	45	36		6.4		0	42
	50	63		2.8			66
	60	58	17	8.0	4.6	0.3	66
	75	98	23	8.0	7.9	0.2	106
	90	134	94	15	12	0.9	150
	100	101		9.9			111
	120	172	92	29	20	1	202
	135	187	115	42	30	3	232
^{58}Ni	30	40	16	1.9	0.97	0	42
	45	70		10		0	80
	50	83		4.2			87
	60	77	33	13	7.5	0.5	90
	75	146	47	11	6.9	0.5	157
	90	171	51	18	14	1	190
	100	200		19			220
	120	230	124	43	33	2	275
	135	243	124	66	49	4	313
	150	235		43			278
^{208}Pb	30	71	24	5.7	4.0	0	77
	45	77		9.8		0	87
	50	111		3.0			114
	60	109	40	15	13	0.8	125
	75	228	73	14	12	1	243
	90	249	100	21	18	1	271
	100	259		11			270
	120	290	116	42	35	10	342
	135	315	62	55	38	7	377
	150	322		30			352

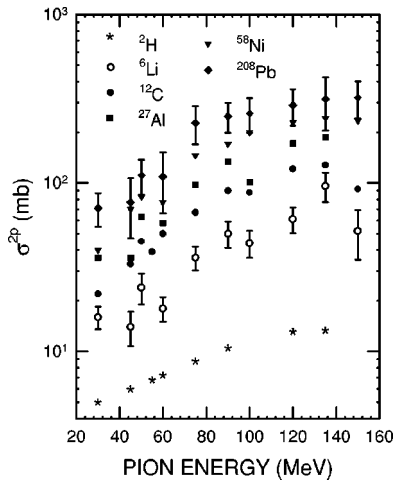

FIG. 15. Inclusive $(\pi^+,2p)$ cross sections σ^{2p} determined in this work. Also shown are the results of Ref. [8] for 50, 100, and 150 MeV corrected for higher multiplicity contributions. Results measured here for deuterium are shown for comparison. Uncertainties are shown for the ^{6}Li and ^{208}Pb data; in general, uncertainties are less than 25%.

MeV appear to be higher than the current measurements by perhaps 10–20 %, but this difference lies within the uncertainties of the two measurements.

In an exercise to test the effect of a 25 MeV proton detection threshold on the proton spectra measured here, raw data from the experiment were replayed with a software gate which simulated an additional 15 MeV applied to the threshold for any measured proton for the $T_\pi = 90$ MeV data. The resulting measured $3p$ spectrum was reduced by a factor of 1.9. Monte Carlo simulations of this same threshold effect yielded a factor of 1.7, in good agreement with the results of the test data and yielding cross sections in agreement with those measured here.

Both these measurements and those of Ransome *et al.* [5,6,8] below resonance show the same systematic behavior for the $3p$ inclusive cross sections, a sharp rise with energy

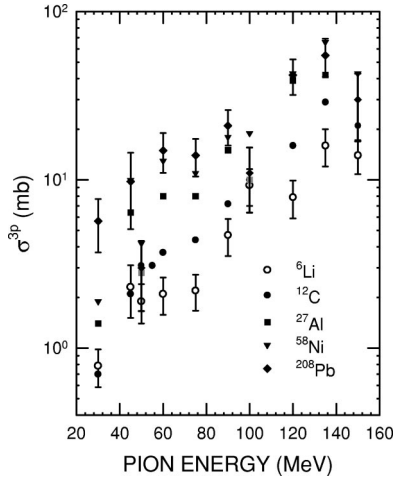

FIG. 16. Inclusive $(\pi^+,3p)$ cross sections σ^{3p} determined in this work. Also shown are the results of Ref. [8] for 50, 100, and 150 MeV. In general, uncertainties are less than 25%.

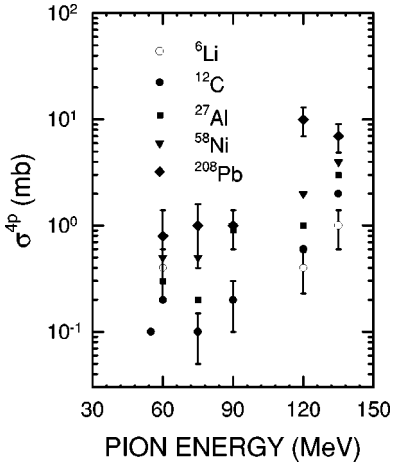

FIG. 17. Inclusive (π^+,4p) cross sections σ^{4p} determined in this work. Contributions from final states with five or more protons are assumed negligible. Also shown are the results of Ref. [8] for 50, 100, and 150 MeV. Uncertainties are discussed in the text.

roughly equivalent to that seen for the $2p$ inclusive cross sections. In the region from $T_\pi = 200$ to 500 MeV studied by Jones *et al.* [11], however, the increase is less marked. The $3p$ cross sections become nearly constant for ^{12}C and increase from a factor of about 2 for ^{58}Ni to a factor of about 4 for ^{208}Pb. At the highest energies, the $3p$ cross sections are about 35% of the $2p$ cross sections. Thus, throughout the energy range from 30 to 500 MeV, the $3p$ cross sections rise in importance relative to the $2p$ cross sections quite gradually, from 10–15 % of the $2p$ cross sections in the region studied here to about twice that fraction at 500 MeV.

The LADS Collaboration has also performed a series of systematic studies on nuclei heavier than helium [32]. Those measurements have been broken down into cross sections for individual final states similar to those reported here. Comparisons with those results are given in Tables IV and V. The

TABLE III. Estimated QDA cross sections in mb, with uncertainties as discused in the text. Unperturbed QDA cross sections σ_{2p}^{QDA} and the additional QDA strength σ_{2p1n}^{QDA} are described in Sec. IV. Estimated total QDA cross sections σ^{QDA} are listed in column 5.

Nucleus	T_π(MeV)	σ_{2p}^{QDA}	σ_{2p1n}^{QDA}	σ^{QDA}
^{6}Li	30	13	0.30	13
	60	16	0.88	17
	75	24	4.7	29
	90	34	1.8	36
	120	41	3.6	45
	135	58	14	72
^{12}C	30	9.1	3.1	12
	60	27	6.6	34
	75	24	7.9	32
	90	34	4.9	39
	120	39	6.2	45
	135	40	4.8	45
^{27}Al	30	7.7	7.6	15
	60	11	12	23
	75	17	32	49
	90	21	8.6	30
	120	16	33	48
^{58}Ni	30	18	6.2	25
	60	17	17	34
	75	20	29	48
	90	26	24	50
	120	27	12	39
	135	28	27	55
^{208}Pb	30	16	12	30
	60	17	16	33
	75	22	25	47
	90	27	27	53
	135	46	18	64

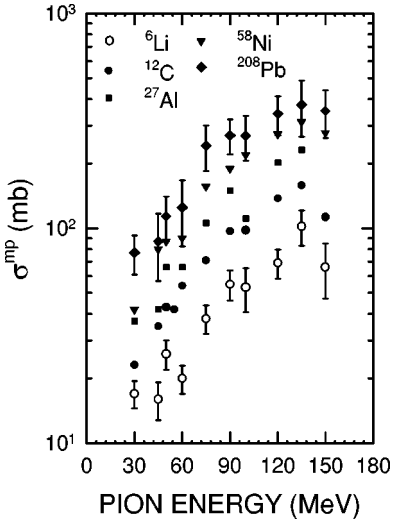

FIG. 18. Total cross sections for pion absorption resulting in two or more protons in the final state σ^{mp} as inferred from the data shown in Figs. 15, 16, and 17.

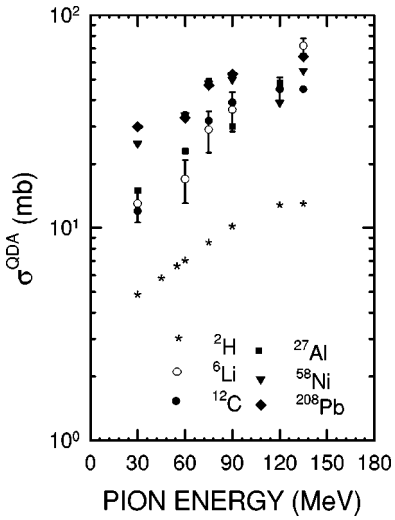

FIG. 19. Total cross section estimates for quasideuteron pion absorption σ^{QDA} as discussed in the text.

TABLE IV. Results from this work for ^{12}C at 120 MeV compared with results from LADS [32] for ^{14}N at 118 MeV. Cross sections are in mb with uncertainties in parentheses. Estimates for single proton and deuteronic final states for this work are discussed in Sec. VI B.

Cross section component	^{12}C (present work)	^{14}N (LADS)
$2p1n$	37(7)	28(3)
$2p$ inclusive	121(30)	103(6)
$3p1n$	12(3)	5(1)
$3p$ inclusive	16(4)	17(1)
$4p$	0.6(3)	0.7(1)
Multiproton	138(30)	121(6)
No proton	2 (est)	—
Single proton	34 (est)	41(4)
Deuteron	31 (est)	21(2)
Total	205(50) (est)	182(10)

LADS results given in [32] have not been corrected for detector threshold or acceptance. Since the LADS detector subtends over 95% of the total solid angle [33], primarily the threshold corrections are of concern; those will increase the cross sections reported for LADS somewhat. Nonetheless, such corrections are probably smaller than the uncertainties in the cross sections measured here and compared in Tables IV and V.

Because single charged particle and deuteron final states were not measured here, those contributions are estimated as discussed in the next section. For those cross sections for which final states are reported here, the agreement between these two sets of measurements using very different techniques is reasonably good. Estimates used here for single proton and deuteronic final states are also in reasonable agreement with the LADS results.

B. Comparison with total absorption cross sections

There are considerable differences between the total multiproton final state cross sections σ^{mp} measured here and earlier measurements of the total pion absorption cross section σ_{abs} [31,34,35]. This discrepancy can be seen in Table VI, where the comparison is made for pion energies at and above 75 MeV. While the σ^{mp} reported here for the lightest nuclei are in rough agreement with σ_{abs}, σ^{mp} becomes progressively lower than σ_{abs} with increasing A. A similar disagreement was seen in the earlier BGO Ball work [5,6]. Further, as noted above, the total multiproton emission absorption cross sections have a smaller mass dependence $A^{0.46}$ than earlier estimates of $A^{0.7}$ [31] for the total absorption cross sections.

TABLE V. Results from this work for ^{27}Al and ^{58}Ni at 120 MeV compared to with results from LADS [32] for ^{40}Ar at 118 MeV, as in Table IV.

Cross section component	^{27}Al (this work)	^{40}Ar (LADS)	^{58}Ni (this work)
$2p1n$	92(18)	69(6)	124(24)
$2p$ inclusive	172(43)	194(12)	230(58)
$3p1n$	20(5)	7(1)	33(8)
$3p$ inclusive	29(7)	25(2)	43(11)
$4p$	1.0(5)	0.8(2)	2(1)
Multiproton	202(44)	220(12)	275(59)
No proton	10 (est)	—	24 (est)
Single proton	85 (est)	133(11)	156 (est)
Deuteron	52 (est)	42(4)	80 (est)
Total	350(90) (est)	393(21)	540(135) (est)

TABLE VI. Estimated total absorption cross sections σ_{est} as discussed in Sec. VI B compared with total absorption cross sections σ_{abs} from previous measurements. The σ^{mp} are from Table II. Also given are estimates of the zero-proton σ^{0p}, single-proton σ^{1p}, and deuteronic final state σ^{d} contributions as discussed in Sec. VI B. Pion kinetic energy T_π is in MeV. Cross sections are in mb, with uncertainties given in parentheses.

Nucleus	T_π	σ^{mp}	σ^{0p}	σ^{1p}	σ^{d}	σ_{est}	σ_{abs}
^{12}C	90	97	2	29	23	150(40)	109(20)[a]
	120	138	2	34	31	205(50)	166(26)[a]
^{27}Al	75	106	8	63	31	210(50)	260(52)[b]
	90	150	10	80	42	280(70)	282(56)[b]
							252(40)[a]
	120	202	10	85	52	350(90)	256(52)[b]
							340(50)[a]
^{58}Ni	75	157	23	124	54	360(90)	521(104)[b]
	90	190	23	132	61	410(100)	552(110)[b]
							421(70)[a]
	120	275	24	156	80	540(135)	552(110)[b]
							527(74)[a]
^{208}Pb	75	243	133	388	135	900(225)	970(185)[b]
	90	271	133	392	140	940(235)	1047(210)[b]
							1659(655)[a]
	120	342	122	394	151	1010(250)	1045(210)[b]
							1235(230)[b]

[a]Reference [31].
[b]Reference [34].

The reason for this discrepancy may be attributed to that portion of the total absorption cross section which does not involve multiproton final states. As noted earlier, measurements with deuterons in the final state could not be corrected for reaction and target losses with precision. Previous measurements [8,9,11,36] suggest that deuteron final states comprise from 10% to 25% of the total pion absorption cross section for these energies, with the average being roughly 15%. For the present discussion, we assume that 15% of the cross section is attributable to deuterium final states. Furthermore, in this work, contributions due to single-proton or no-proton final states were not measured. Such states may be due to nucleon rescattering following pion absorption in which a proton transfers sufficient energy to a neutron such that the proton falls below the detection threshold or does not emerge at all from the nucleus. Such medium effects are not included in the Monte Carlo simulations described above.

When these contributions are taken into consideration, the total absorption cross sections could be substantially different from the total multiproton final state absorption cross sections. The difference seen here, then, argues strongly that, in addition to the contribution due to deuteronic final states, a contribution to the pion absorption process is present which results in one or no proton in the final state with one or more neutrons, and that this process grows in importance with mass. Indeed, such a single proton contribution is seen in the LADS results shown in Tables IV and V, accounting for approximately one-fifth of the cross section in nitrogen and one-third that of argon at 118 MeV. For carbon, the bubble chamber work of Bellotti, Cavalli, and Matteuzzi [36] at 130 MeV also found that roughly 12% of the pion absorption cross section resulted in a single-charged-particle track after estimating the background due to charge exchange.

To estimate this missing contribution for our data, we have used the following approach. The quasioptical model of Vicente Vacas and Oset [37] describes pion absorption through $2NA$ and $3NA$ and includes the effects of nucleon propagation through the nuclear medium. Final states modeled by this approach include $(\pi,N),(\pi,2N)$, and $(\pi,3N)$, and the results reported in Ref. [37] provide a remarkably good description of the final state decompositions. However, the model does not explicitly account for some of the features of the absorption process, such as energy lost to breakup of the residual nucleus into larger fragments, excitation of the residual nucleus, or the separation energy of the outgoing nucleons.

We have incorporated the Vicente Vacas–Oset model into a simulation of the BGO Ball response to pion absorption on the various target and energy combinations measured in this work. By incorporating this model into such a simulation, the predictions of the model for the relative strengths of various final states and the shape of the summed proton energy distributions can be compared with the results found here. The unmodified model was found to overestimate the ratio of two- to three-proton final states, and yielded summed proton energy spectra qualitatively different from those observed here. However, with the addition of an empirical 20–25 MeV energy loss per nucleon to account for some of the omissions in the model noted above, and ignoring those nucleons whose energy fell below the energy loss per nucleon threshold, the model gave a reasonable estimate of the two- to three-proton cross section ratios. For instance, the modified model yielded two- to three-proton ratios within about 20% of those observed for Ar at 118 MeV by LADS. Furthermore, the modified model yielded good qualitative agreement with the observed summed proton energy spectra.

The resulting total absorption cross section estimates based on the measurements made here incorporating this missing strength and a 15% deuteron contribution are given in Tables IV–VI. The uncertainties on the missing strength and deuteron contribution are estimated to be on the order of 20%. The predictions for the cross sections for single-charged-particle final states and deuteronic final states for nuclei studied here are in excellent systematic agreement with the measurements obtained by the LADS Collaboration for nitrogen and argon [32]. The predicted contribution of about 16% for single proton final states in ^{12}C at 120 MeV is similar to the 12% result noted above from Bellotti, Cavalli, and Matteuzzi [36] and the 20% result seen in Table IV from the LADS data for ^{14}N. Furthermore, it is seen in Table VI that these additional contributions when added to the multiproton pion absorption cross sections measured here result in estimated total absorption cross sections from this work generally in agreement with those measured by Ashery *et al.* [31] and Nakai *et al.* [34].

We note that our estimates are systematically somewhat lower than the Ashery *et al.* measurements for Ni and Pb. A similar discrepancy was noted in Ref. [32], which suggested all of the total absorption cross sections reported in Ashery *et al.* are perhaps 25% too large. Reference [32] has noted that part of this discrepancy may be due to the underestimation of the single-charge-exchange (SCX) contribution in the earlier work, as a comparison between Refs. [31] and [38] indicates. Using the newer SCX values lowers the Ashery *et al.* total cross sections by about 10% and brings them in better agreement with the results from the results of Nakai *et al.*, the LADS results, and those estimated here.

As noted previously [8], the earlier BGO Ball results at 50 MeV are very low compared with the results of Navon *et al.* [35] and Nakai *et al.* [34]. Since this energy lies below the applicability of the Vicente Vacas–Oset model, no firm conclusion as to whether this discrepancy might be attributable to the single-proton channel can be made. However, the general agreement seen in the comparisons at higher energy suggests that some of the discrepancy might be be due to such an explanation.

While the Vicente Vacas–Oset formalism is not applicable to nuclei as light as ^{6}Li, the total absorption cross sections for ^{6}Li are most likely identical to the multiproton cross sections measured in this work since the contribution from single charged particle emission was found to be only about 10% in the case for ^{12}C.

The general agreement found in these comparisons provides a confirmation of the validity of the optical model of Vicente Vacas and Oset, and adds support to the data presented here. The agreement illustrated in Tables IV–VI suggests that, at the highest energies measured here, the contribution to the pion absorption cross section from final states with fewer than two protons increases from about one-tenth of the cross section in ^{12}C to about one-third in nickel, to about one-half of the cross section for ^{208}Pb. The variation in the contribution from such final states could be attributable to NN interactions within the larger nuclei and the neutron excess of the larger mass nuclei. This variation in the relative strength of final states with fewer than two protons might also be couched in terms of initial and final state interactions during the pion absorption process, but the angular resolution of the BGO Ball here and the limited statistics when the data are broken up into rings are not sufficient to clarify this issue.

C. Role of quasideuteron absorption

The results of this work provide some insight into the mass and energy dependences of the QDA process. Without

considering initial state interactions (ISIs) and final state interactions (FSIs), the estimated total contribution (unperturbed and $2p1n$) from QDA in the light nucleus ^{6}Li dominates the multiproton final state pion absorption cross section, going from around 100% at 30 MeV down to approximately 65% at 135 MeV. In the heavier nuclei, however, the total contribution from QDA is less significant; QDA accounts for between 40% and 60% at 30 MeV and down to between 15% and 25% in nuclei from lead to carbon, respectively, with QDA decreasing in importance with increasing nuclear mass.

Several works have estimated QDA cross sections, and the results found here are in general agreement with those, despite the markedly different methods and models assumed in each case. In ^{12}C, Yokota *et al.* [39] determined what would correspond to the unperturbed QDA contribution measured here to be on the order of 15 mb at 70 MeV using their (π^+,pp) data, lower than the values obtained here but within uncertainties. At 130 MeV, the same work obtained 16 mb, about half of that determined here. However, the Yokota *et al.* work used a two-Gaussian deconvolution procedure for the angular distributions which most likely underestimates the true QDA cross section. This assessment receives support from the more recent work by Huber *et al.* [20]. Those authors have estimated QDA cross sections at 100 MeV for ^{12}C, and the results found here are in general agreement with those. The cross section most closely related to the unperturbed QDA cross section measured here was their two-nucleon absorption result, labeled as *''2NA*''* in their paper, found to be about 29 mb, while the corresponding unperturbed QDA cross section measured here at 90 MeV was 34 mb. Their *''2NA-like''* cross section is most comparable to σ^{QDA} here; their result at 100 MeV was 38 mb, while the result here was 39 mb. This agreement, despite various approaches used, indicates the degree to which the kinematical constraints imposed resemble each other and provide some confirmation for the robustness of the estimates.

Several studies have been performed below resonance on ^{16}O aimed at identifying the importance of QDA [9,40–43]. Comparisons with those results can be made using the results for ^{12}C reported here. If a total pion absorption cross section for ^{12}C at 60 MeV is estimated by the addition of 15% of the cross section for deuteronic final states and about 10% for $1pX$ contributions, the ratio of the total QDA cross section obtained here to the total pion absorption cross section at 60 MeV is about 50%, in agreement with the large acceptance detector result of (55 ± 5)% reported in Ref. [9]. The same ratio for the observed QDA cross section at 120 MeV for our ^{12}C data would be about 25%, nearly the same as the approximately 30% observed (i.e., without estimated final state interaction corrections) in Refs. [42,43] for 115 MeV, and roughly consistent with the value of (38 ± 10)% found in Ref. [40] for the same energy using similar equipment but different assumptions about extrapolations to unmeasured regions of phase space. Considering the very different techniques used, the agreement is quite good.

An estimate of the effective number of quasideuterons participating in the absorption process n_D can be made using the QDA cross section estimates obtained here and the free $\pi^+ d \rightarrow pp$ reaction cross section. The ratios are roughly constant with energy for each nucleus, suggesting that the effective number of quasideuterons also remains approximately constant with energy for each nucleus. The averages over all energies for each nucleus were 3.7 ± 1.2, 3.9 ± 0.8, 4.0 ± 1.2, 4.9 ± 1.0, and 5.7 ± 0.6 for ^{6}Li, ^{12}C, ^{27}Al, ^{58}Ni, and ^{208}Pb, respectively.

For ^{6}Li, Zhang [44] calculated $n_D=3.8$ as the total number of possible quasideuterons which could exist based on $1s$-$2p$ shell model configurations coupled to the deuteron angular momentum and isospin. That number agrees with the average found here for ^{6}Li. The n_D values determined by Yokota *et al.* [39] using their (π^+,pp) data for ^{6}Li and ^{12}C are considerably lower than the estimates found here, again probably due to the deconvolution process used, but also due to the restriction of their estimate to what would be unperturbed QDA here. Their values for n_D using the (π^+,p) channel, on the other hand, are about a factor of 2 higher than the values reported here. If their (π^+,pp) and (π^+,p) values for n_D are viewed as lower and upper limits, respectively, the values found here fall into that range. While Huber *et al.* did not report n_D values, the agreement of comparable cross sections in this work with theirs suggests comparable values of n_D.

Not surprisingly, the average effective number of quasideuterons grows with increasing mass A, suggestive of the greater likelihood of finding quasideuterons in the heavier nuclei. This growth, however, is markedly less than might be expected by simple statistical estimates of the possible number of quasideuterons. Some of this difference, particularly in the largest nuclei, is likely due to shadowing, though some portion may simply be due to the effects of FSI obscuring the QDA signature used here.

D. $2p1n$ and $3p1n$ strength in positive pion absorption

The summed proton energy spectra give considerable evidence for the presence of two-proton final states containing one or more neutrons. While in light nuclei the lower-energy region of the summed proton spectra is dominated by $2p1n$ contributions, in heavier nuclei a $2p2n$ contribution is suggested by the phase space simulations. As noted above, there is considerable ambiguity in ascertaining the strength for neutron multiplicities above 1, and only $2p1n$ exclusive results are reported here. However, as suggested in Refs. [8] and [11], the low summed proton energy region for heavy nuclei likely contains contributions from $2p2n$ final states and from final states with higher neutron multiplicities.

Curiously, recent measurements [21] on ^{12}C using the CHAOS spectrometer [45] found no $2p1n$ strength whatsoever above resonance. While their spectra are very similar to those in previous BGO Ball studies [8] and qualitatively similar to those obtained here, their simulations indicated that the region determined to contain $2p1n$ strength here and in Ref. [8] was instead due to contributions from the $3p$ inclusive yield in which one of the protons was missed. This inference was based on extrapolating their observed $3p$

yields to their observed $2p$ measurements in a manner similar to that performed here.

Since the present measurements cover almost 90% of the available solid angle versus about 10% in the case of CHAOS, the uncertainties associated with extrapolating the $3p$ measurements to reduce the observed $2p$ spectra are considerably less for the present work. In particular, the extrapolation to noncoplanar events is very sensitive to the model chosen to generate those events. The greater solid angle subtended here would better ascertain the full strength of contributions involving three or more nucleons than the more limited coverage available in CHAOS and, thus, provide additional support to the inference of $2p1n$ strength made here.

As noted above, the $3p1n$ contributions dominate the observed $3p$ summed proton energy spectra. While the CHAOS measurements [21] are at energies considerably above the present work, some comparisons can be examined for the strength of the $3p1n$ contribution. The CHAOS measurements yield a cross section for four nucleons participating in the pion absorption process of around 25 mb. Since the $3p$ inclusive cross sections continue to rise by about a factor of 2 between the highest energy studied here (135 MeV) and 200 MeV (above which the $3p$ cross section remains roughly constant [11]), their results would be roughly consistent with scaling the results obtained here for σ_{excl}^{3p1n} cross section, 13 mb, by the same factor of two.

At these lower energies the $3p1n$ phase space is the dominant contribution to the cross sections when more than two protons are detected in the BGO Ball. The results here indicate this component increases rapidly with energy. Similarly, Jones *et al.* [11] have also reported that the importance of the $3p$ phase space distributions increases even more at higher energies. Magnitudes of the $^{12}C(\pi^+,3p1n)$ total cross sections measured here are comparable to the magnitudes of cross sections for the $^4He(\pi^+,3p1n)$ reaction measured by Balestra, *et al.* [46]. Those values were 11 mb and 12 mb at 120 MeV and 145 MeV, respectively. Recent measurements of three nucleon pion absorption cross sections on ^{3}He and ^{4}He [18] are somewhat smaller than the results of Balestra *et al.* Thus, the ^{3,4}He and ^{12}C measurements reported elsewhere suggest that the magnitude of the $3p1n$ contribution increases with A as seen here.

VII. CONCLUSIONS

In conclusion, a thorough systematic study of the energy and mass dependence of pion absorption leading to two or more protons in the final state for energies below resonance has been made with a large solid angle detector, providing the first detailed study of important inclusive components of the reaction mechanism. With respect to the mass dependence for pion absorption, the results obtained here indicate the cross sections for energies below the $\Delta(1232)$ resonance are dominated by the inclusive $(\pi^+,2p)$ channel. The mass dependence for that channel is described quite well by $A^{0.49}$, or approximately $\sqrt{A}$, as was the mass dependence for the cross sections for inclusive $(\pi^+,3p)$.

The energy dependence for the $(\pi^+,2p)$ cross sections is somewhat steeper than that observed for $\pi^+ d \rightarrow pp$, suggesting the presence of components other than QDA for that channel. The energy dependence of the cross sections for inclusive $(\pi^+,3p)$ and $(\pi^+,4p)$ rises by over an order of magnitude in the energy range studied. Nonetheless, the $3p$ cross sections are approximately 10–20 % of the $2p$ cross sections throughout the energy region studied here.

Comparisons of these results with past BGO Ball and LADS results show good agreement. The mass dependence of the $2p$ inclusive cross sections determined here is also consistent with the results of Favier *et al.* at 165 MeV [30]. However, the cross sections of Favier *et al.* and those measured here do not include contributions from single proton final states. When such states are simulated with the Vicente Vacas–Oset optical model formalism [37] and folded into the measurements made here along with an additional contribution of 15% for deuteronic final states, the total cross section estimates obtained are consistent with previous measurements [31,34,35]. These estimates indicate that a portion of the total cross section for heavy nuclei, growing with A, results in final states with fewer than two protons. Such a rise may be attributable to the greater neutron excess for larger nuclei as well as the larger nuclear volume for those nuclei.

The importance of quasideuteron absorption relative to other pion absorption mechanisms decreases with A. The effective number of quasideuterons for a given nucleus remains roughly constant within the energy range studied here. The effective number of quasideuterons increases only by a factor of about 2 from ^{6}Li to ^{208}Pb, a much smaller increase than a combinatorial estimate would suggest. The energy dependence of this component of the pion absorption mechanism still retains the shape of the fundamental $\pi^+ d \rightarrow pp$ process.

ACKNOWLEDGMENTS

This work was supported by the U.S. National Science Foundation, the U.S. Department of Energy, and NATO Collaborative Research Grant No. CRG890498. The authors thank Eulogio Oset and Manuel J. Vicente Vacas for useful correspondence with respect to the interpretation of the data presented here.

[1] D. Ashery and J. P. Schiffer, Annu. Rev. Nucl. Part. Sci. **36**, 213 (1986).
[2] H. J. Weyer, Phys. Rep. **195**, 295 (1990).
[3] C. H. Q. Ingram, Nucl. Phys. **A553**, 573c (1993).
[4] W. J. Burger, E. Beise, S. Gilad, R. P. Redwine, P. G. Roos, N. S. Chant, H. Breuer, G. Ciangaru, J. D. Silk, G. S. Blanpied, B. M. Preedom, B. G. Ritchie, M. Blecher, K. Gotow, D. M. Lee, and H. Ziock, Phys. Rev. C **41**, 2215 (1990).
[5] R. D. Ransome, V. R. Cupps, S. Dawson, R. W. Fergerson, A. Green, C. L. Morris, J. A. McGill, J. R. Comfort, B. G. Ritchie, J. R. Tinsley, J. D. Zumbro, R. A. Loveman, P. C. Gugelot, D. L. Watson, and C. Fred Moore, Phys. Rev. Lett. **64**, 372 (1990).
[6] R. D. Ransome, V. R. Cupps, S. Dawson, R. W. Fergerson, A.

Green, C. L. Morris, J. A. McGill, J. R. Comfort, B. G. Ritchie, J. R. Tinsley, J. D. Zumbro, R. A. Loveman, P. C. Gugelot, D. L. Watson, and C. Fred Moore, Phys. Rev. C **42**, 1500 (1990).

[7] M. K. Jones, B. G. Ritchie, C. L. Morris, R. D. Ransome, J. A. McGill, D. L. Watson, C. Fred Moore, D. Clayton, K. Pujara, I. Brown, and P. Campbell, Phys. Lett. B **278**, 419 (1992).

[8] R. D. Ransome, C. L. Morris, V. R. Cupps, R. W. Fergerson, J. A. McGill, D. L. Watson, J. D. Zumbro, B. G. Ritchie, J. R. Comfort, J. R. Tinsley, R. A. Loveman, S. Dawson, A. Green, P. C. Gugelot, and C. Fred Moore, Phys. Rev. C **45**, R509 (1992).

[9] Th. S. Bauer, R. Hamers, P. Boberg, H. Breuer, R. van Dantzig, J. Konijn, C. T. A. M. de Laat, Y. Lefevere, A. Taal, J. L. Visschers, and R. Ykema, Phys. Rev. C **46**, R20 (1992).

[10] R. D. Ransome, C. L. Morris, M. K. Jones, B. G. Ritchie, D. L. Watson, J. A. McGill, K. Pujara, D. B. Clayton, I. Brown, P. Campbell, and C. Fred Moore, Phys. Rev. C **46**, 273 (1992).

[11] M. K. Jones, R. D. Ransome, V. R. Cupps, R. W. Fergerson, C. L. Morris, J. A. McGill, J. D. Zumbro, J. R. Comfort, B. G. Ritchie, J. R. Tinsley, P. C. Gugelot, and C. Fred Moore, Phys. Rev. C **48**, 2800 (1993).

[12] T. Alteholz, D. Androić, G. Backenstoss, D. Bosnar, H. Breuer, A. Brković, H. Döbbeling, T. Dooling, W. Fong, M. Furić, P. A. M. Gram, N. K. Gregory, J. P. Haas, A. Hoffart, C. H. Q. Ingram, A. Klein, K. Koch, J. Köhler, B. Kotliński, M. Kroedel, G. Kyle, A. Lehmann, Z. N. Lin, G. Mahl, A. O. Mateos, K. Michaelian, S. Mukhopadhyay, T. Petković, R. P. Redwine, D. Rowntree, R. Schumacher, U. Sennhauser, N. Šimičević, F. D. Smit, G. van der Steenhoven, D. R. Tieger, R. Trezeciak, H. Ullrich, M. Wang, M. H. Wang, H. J. Weyer, M. Wildi, and K. E. Wilson, Phys. Rev. Lett. **73**, 1336 (1994).

[13] H. Breuer, M. G. Khayat, F. Adimi, B. S. Flanders, M. A. Khandaker, P. G. Roos, D. Zhang, Th. S. Bauer, J. Konijn, C. T. A. M. de Laat, G. S. Kyle, S. Mukhopadhyay, M. Wang, and R. Tacik, Phys. Rev. C **49**, R2276 (1994).

[14] Z. Papandreou, G. M. Huber, G. J. Lolos, J. C. Cormier, E. L. Mathie, S. I. H. Naqvi, D. F. Ottewell, R. Tacik, P. L. Walden, G. Jones, R. P. Trelle, X. Aslanoglou, and D. L. Humphrey, Phys. Rev. C **51**, R2862 (1995).

[15] G. Backenstoss, D. Bosnar, H. Breuer, H. Döbbeling, T. Dooling, M. Furić, P. A. M. Gram, N. K. Gregory, A. Hoffart, C. H. Q. Ingram, A. Klein, K. Koch, J. Köhler, B. Kotliński, M. Kroedel, G. Kyle, A. Lehmann, A. O. Mateos, K. Michaelian, T. Petković, R. P. Redwine, D. Rowntree, U. Sennhauser, N. Šimičević, R. Trezeciak, H. Ullrich, M. Wang, M. H. Wang, H. J. Weyer, M. Wildi, and K. E. Wilson, Phys. Lett. B **379**, 60 (1996).

[16] D. Androić, G. Backenstoss, D. Bosnar, H. Breuer, A. Brković, H. Döbbeling, T. Dooling, M. Furić, P. A. M. Gram, N. K. Gregory, A. Hoffart, C. H. Q. Ingram, A. Klein, K. Koch, J. Köhler, B. Kotliński, M. Kroedel, G. Kyle, A. Lehmann, A. O. Mateos, K. Michaelian, T. Petković, R. P. Redwine, D. Rowntree, U. Sennhauser, N. Šimičević, R. Trezeciak, H. Ullrich, M. Wang, M. H. Wang, H. J. Weyer, M. Wildi, and K. E. Wilson, Phys. Rev. C **53**, R2591 (1996).

[17] G. J. Lolos, G. M. Huber, E. L. Mathie, S. I. H. Naqvi, Z. Papandreou, D. F. Ottewell, P. L. Walden, G. Jones, X. Aslanoglou, and J. L. Visschers, Phys. Rev. C **54**, 211 (1996).

[18] A. Lehmann, D. Androić, G. Backenstoss, D. Bosnar, H. Breuer, H. Döbbeling, T. Dooling, M. Furić, P. A. M. Gram, N. K. Gregory, A. Hoffart, C. H. Q. Ingram, A. Klein, K. Koch, J. Köhler, B. Kotliński, M. Kroedel, G. Kyle, A. O. Mateos, K. Michaelian, T. Petković, M. Planinić, R. P. Redwine, D. Rowntree, U. Sennhauser, N. Šimičević, R. Trezeciak, H. Ullrich, M. Wang, M. H. Wang, H. J. Weyer, M. Wildi, and K. E. Wilson, Phys. Rev. C **55**, 2931 (1997).

[19] A. Lehmann, D. Androić, G. Backenstoss, D. Bosnar, H. Breuer, A. Brković, H. Döbbeling, T. Dooling, M. Furić, P. A. M. Gram, N. K. Gregory, A. Hoffart, C. H. Q. Ingram, A. Klein, K. Koch, J. Köhler, B. Kotliński, M. Kroedel, G. Kyle, A. O. Mateos, K. Michaelian, T. Petković, M. Planinić, R. P. Redwine, D. Rowntree, U. Sennhauser, N. Šimičević, R. Trezeciak, H. Ullrich, M. Wang, M. H. Wang, H. J. Weyer, M. Wildi, and K. E. Wilson, Phys. Rev. C **56**, 1872 (1997).

[20] G. M. Huber, G. J. Lolos, Z. Papandreou, J. C. Cormier, E. L. Mathie, S. I. H. Naqvi, D. F. Ottewell, P. L. Walden, G. Jones, R. P. Trelle, X. Aslanoglou, and J. L. Visschers, Nucl. Phys. **A624**, 623 (1997).

[21] R. Tacik, F. Farzanpay, E. L. Mathie, P. Amaudruz, J. T. Brack, L. Felawka, R. Meier, D. Ottewell, G. R. Smith, G. Hofman, M. Kermani, S. McFarland, K. Raywood, M. Sevior, F. Bonutti, P. Camerini, N. Grion, R. Rui, and E. F. Gibson, Phys. Rev. C **57**, 1295 (1998).

[22] B. Kotlinski, D. Androić, G. Backenstoss, D. Bosnar, H. Breuer, H. Döbbeling, T. Dooling, M. Furić, P. A. M. Gram, N. K. Gregory, A. Hoffart, C. H. Q. Ingram, A. Klein, K. Koch, J. Köhler, M. Kroedel, G. Kyle, A. Lehmann, A. O. Mateos, K. Michaelian, T. Petković, M. Planinić, R. P. Redwine, D. Rowntree, U. Sennhauser, N. Šimičević, R. Trezeciak, H. Ullrich, H. J. Weyer, M. Wildi, and K. E. Wilson, Eur. Phys. J. A **1**, 435 (1998).

[23] A. O. Mateos, D. Androić, G. Backenstoss, D. Bosnar, H. Breuer, H. Döbbeling, T. Dooling, M. Furić, P. A. M. Gram, N. K. Gregory, A. Hoffart, Q. Ingram, A. Klein, K. Koch, J. Köhler, B. Kotliński, M. Kroedel, G. Kyle, A. Lehmann, K. Michaelian, T. Petković, M. Planinić, R. P. Redwine, D. Rowntree, U. Sennhauser, N. Šimičević, R. Trezeciak, H. Ullrich, M. Wang, M. H. Wang, H. J. Weyer, M. Wildi, and K. E. Wilson, Phys. Rev. C **58**, 942 (1998).

[24] R. A. Giannelli, Ph.D. thesis, Arizona State University, 1995 (unpublished).

[25] R. L. Burman, R. L. Fulton, and M. Jakobson, Nucl. Instrum. Methods **131**, 29 (1975).

[26] E. V. Beck and J. C. Beck, J. Undergrad. Res. Phys. **12**, 57 (1994).

[27] B. G. Ritchie, Phys. Rev. C **44**, 533 (1991).

[28] L. C. Smith, R. C. Minehart, D. Ashery, E. Piasetsky, M. Moinester, I. Navon, D. F. Geesaman, J. P. Schiffer, G. Stephens, B. Zeidman, S. Levinson, S. Mukhopadhyay, R. E. Segal, B. Anderson, R. Madey, J. Watson, and R. R. Whitney, Phys. Rev. C **40**, 1347 (1989).

[29] Neven Simičević, and Arthur Mateos, Phys. Rev. C **51**, 797 (1995).

[30] J. Favier, T. Bressani, G. Charpak, L. Massonet, W. E. Meyerhof, and C. Zupanic, Nucl. Phys. **A169**, 540 (1971).

[31] D. Ashery, I. Navon, G. Azuelos, H. K. Walter, H. J. Pfeiffer, and F. W. Schlepütz, Phys. Rev. C **23**, 2173 (1981).

[32] D. Rowntree, D. Androić, G. Backenstoss, D. Bosnar, H. Breuer, T. Dooling, M. Furić, P. A. M. Gram, N. K. Gregory, A. Hoffart, C. H. Q. Ingram, A. Klein, K. Koch, J. Köhler, B. Kotliński, M. Kroedel, G. Kyle, A. Lehmann, A. O. Mateos, K. Michaelian, T. Petković, M. Planinić, R. P. Redwine, U. Sennhauser, N. Šimičević, R. Trezeciak, H. J. Weyer, M. Wildi, and K. E. Wilson, Phys. Rev. C **60**, 054610 (1999).

[33] T. Altehotz, D. Androić, G. Backenstoss, D. Bosnar, H. Breuer, A. Brković, H. Döbbeling, T. Dooling, W. Fong, M. Furić, P. A. M. Gram, N. K. Gregory, J. P. Haas, A. Hoffart, C. H. Q. Ingram, A. Klein, K. Koch, J. Köhler, B. Kotliński, M. Kroedel, G. Kyle, A. Lehmann, Z. N. Lin, G. Mahl, A. O. Mateos, K. Michaelian, S. Mukhopadhyay, T. Petković, M. Planinić, R. P. Redwine, D. Rowntree, R. Schumacher, U. Sennhauser, N. Šimičević, F. D. Smit, G. van der Steenhoven, D. R. Tieger, R. Trezeciak, H. Ullrich, M. Wang, M. H. Wang, H. J. Weyer, M. Wildi, and K. E. Wilson, Nucl. Instrum. Methods Phys. Res. A **373**, 374 (1996).

[34] N. Nakai, T. Kobayashi, T. Numao, T. A. Shibata, and K. Masutani, Phys. Rev. Lett. **44**, 1446 (1980).

[35] I. Navon, D. Ashery, J. Alster, G. Azuelos, B. M. Barnett, W. Gyles, R. R. Johnson, D. R. Gill, and T. G. Masterson, Phys. Rev. C **28**, R2548 (1983).

[36] E. Bellotti, D. Cavalli, and C. Matteuzzi, Nuovo Cimento **18**, 75 (1973).

[37] M. J. Vicente Vacas and E. Oset, Nucl. Phys. **A568**, 855 (1994).

[38] D. Ashery, D. F. Geesaman, R. J. Holt, H. E. Jackson, J. R. Speht, K. E. Stephenson, R. E. Segel, P. Zupranski, H. W. Baer, J. D. Bowman, M. D. Cooper, M. Leitch, A. Erel, J. Comuzzi, R. P. Redwine, and D. R. Tieger, Phys. Rev. C **30**, 946 (1984).

[39] H. Yokota, S. Igarashi, K. Hama, T. Mori, T. Katsumi, K. Ichimaru, K. Nakayama, R. Chiba, K. Nakai, and J. Chiba, Phys. Rev. C **40**, 270 (1989).

[40] R. A. Schumacher, P. A. Amaudruz, C. H. Q. Ingram, U. Sennhauser, H. Breuer, N. S. Chant, A. E. Feldman, B. S. Flanders, F. Khazaie, D. J. Mack, P. G. Roos, J. D. Silk, and G. S. Kyle, Phys. Rev. C **38**, 2205 (1988).

[41] S. D. Hyman, D. J. Mack, H. Breuer, N. S. Chant, F. Khazaie, B. G. Ritchie, P. G. Roos, J. D. Silk, P. A. Amaudruz, Th. S. Bauer, C. H. Q. Ingram, G. S. Kyle, D. Renker, R. A. Schumacher, U. Sennhauser, and W. J. Burger, Phys. Rev. C **41**, R409 (1990).

[42] D. J. Mack, P. G. Roos, N. S. Chant, S. D. Hyman, F. Khazaie, B. G. Ritchie, J. D. Silk, G. S. Kyle, P. A. Amaudruz, Th. S. Bauer, C. H. Q. Ingram, D. Renker, R. A. Schumacher, U. Sennhauser, and W. J. Burger, Phys. Rev. C **45**, 1767 (1992).

[43] S. D. Hyman, D. J. Mack, P. G. Roos, H. Breuer, N. S. Chant, F. Khazaie, B. G. Ritchie, J. D. Silk, G. S. Kyle, P. A. Amaudruz, Th. S. Bauer, C. H. Q. Ingram, D. Renker, R. A. Schumacher, U. Sennhauser, and W. J. Burger, Phys. Rev. C **47**, 1184 (1993).

[44] D. Zhang, Ph.D. thesis, University of Maryland, 1990 (unpublished).

[45] G. R. Smith, P. A. Amaudruz, J. T. Brack, L. Felawka, A. Gorelov, R. A. Henderson, D. F. Ottewell, P. Vincent, Y. Wu, F. Bonutti, P. Camerini, N. Grion, R. Rui, J. Hoey, G. Hofman, M. Kermani, D. Maas, S. McFarland, K. Raywood, M. E. Servior, E. L. Mathie, R. Tacik, P. Reeve, R. A. Ristinen, E. F. Gibson, R. Meier, and H. M. Staudenmaier, Nucl. Instrum. Methods Phys. Res. A **362**, 349 (1995).

[46] F. Balestra, M. P. Bussa, L. Busso, R. Garfagnini, G. Piragino, C. Guaraldo, A. Maggiora, R. Scrimaglio, I. V. Falomkin, G. B. Pontecorvo, and Yu. A. Shcherbakov, Nucl. Phys. **A340**, 373 (1980).